Lawrence Berkeley National Laboratory

Title
Two-dimensional sp2 carbon—conjugated covalent organic frameworks

Authors
Jin, Enquan
Asada, Mizue
Xu, Qing
et al.

Peer reviewed

REPORT

MOLECULAR FRAMEWORKS

Two-dimensional sp² carbon–conjugated covalent organic frameworks

Enquan Jin,[1] Mizue Asada,[2] Qing Xu,[1] Sasanka Dalapati,[1] Matthew A. Addicoat,[3] Michael A. Brady,[4] Hong Xu,[1,2] Toshikazu Nakamura,[2] Thomas Heine,[5] Qiuhong Chen,[1] Donglin Jiang[1]*

We synthesized a two-dimensional (2D) crystalline covalent organic framework (sp²c-COF) that was designed to be fully π-conjugated and constructed from all sp² carbons by C=C condensation reactions of tetrakis(4-formylphenyl)pyrene and 1,4-phenylenediacetonitrile. The C=C linkages topologically connect pyrene knots at regular intervals into a 2D lattice with π conjugations extended along both x and y directions and develop an eclipsed layer framework rather than the more conventionally obtained disordered structures. The sp²c-COF is a semiconductor with a discrete band gap of 1.9 electron volts and can be chemically oxidized to enhance conductivity by 12 orders of magnitude. The generated radicals are confined on the pyrene knots, enabling the formation of a paramagnetic carbon structure with high spin density. The sp² carbon framework induces ferromagnetic phase transition to develop spin-spin coherence and align spins unidirectionally across the material.

Covalent organic frameworks that exploit conjugated bonding based on sp²-hybridized carbons could create materials with exceptional electronic and magnetic properties (1). To design such an extended structure, the sp² carbon chains must be able to diverge at regular intervals. Such branches should have appropriate geometry for extended π conjugation at the point of knot so that the chains strictly propagate along the x and y directions without blocking the extension of π conjugation. However, amorphous materials will form if the sp² carbon bond formation reactions are irreversible if an in situ structural self-healing process is lacking (2, 3). Thus, designing well-defined two-dimensional (2D) materials and fabricating extended sp² carbon networks with chain propagation along both x and y directions are challenging goals.

We report a topology-directed reticular construction of crystalline sp² carbon–conjugated covalent organic framework (sp²c-COF) by designing a C=C bond formation reaction (Fig. 1A). This reaction (4–7) enables structural self-healing under thermodynamic control during polycondensation. Topology-directed polycondensation (8–13) of C₂-symmetric 1,3,6,8-tetrakis(4-formylphenyl)pyrene (TFPPy) as knots and C₂-symmetric linear 1,4-

phenylenediacetonitrile (PDAN) as linkers under solvothermal conditions (mesitylene/dioxane = 1/5 v/v, 4 M NaOH, 3 days, 90°C) yielded a sp²c-COF. The 2D sp² carbon sheet consists of sp² carbon chains extended along the x and y directions in which pyrene units serve as interweaving registry points that are periodically pitched at 2-nm intervals (Fig. 1, B and D). The 2D sheets crystallize and form stacked layers at 3.58-Å separation, creating ordered pyrene columnar arrays and 1D nanochannels (Fig. 1, C and E). We use the term π conjugation rather than 2D for sp²c-COF because it offers π conjugation along both the x and y directions. Note that a 2D sheet can form, with restricted π conjugation blocked at the point of vertices, as occurs in a 2D polyphenylenevinylene framework knotted by all meta-substituted 1,3,5-phenyl focal units (14). We unexpectedly found that the fully conjugated 2D layers offer the structural base of an sp² carbon lattice that can accommodate exceptionally dense spins and unidirectional spin alignment via ferromagnetic phase transition.

The chemical structure of sp²c-COF was characterized by various analytical methods [see supplementary materials, figs. S1 to S7, and tables S1 and S2 (15)]. Fourier-transform infrared spectroscopy revealed that the peak at 2220 cm⁻¹ had newly appeared for the cyano side group (16) and the peak at 2720 cm⁻¹ assigned to the C–H bond of the aldehyde group was greatly attenuated, indicating the polycondensation between TFPPy and PDAN (fig. S1). Solid-state ¹³C nuclear magnetic resonance spectroscopy of sp²c-COF revealed that the peak at 24.20 parts per million (ppm) for the methylene carbon of PDAN disappeared upon polycondensation, and the peak at 120.44 ppm assigned to PDAN units was shifted to 107.74 ppm (cyano side group), indicating the formation of C=C link-

ages in sp²c-COF (fig. S2). Similar spectral changes were also observed for a model compound (a TFPPy core bound to four PDAN groups) (figs. S1 and S2 and scheme S1A). Field-emission scanning electron microscopy revealed that sp²c-COF and a model compound adopted a belt morphology (fig. S3). Thermogravimetric analysis suggested that sp²c-COF was stable up to 350°C under nitrogen (fig. S4).

The sp²c-COF exhibited powder x-ray diffraction (PXRD) peaks at 3.6°, 5.2°, 5.9°, 7.3°, 11.2°, 11.8°, 14.2°, and 24.7°, which were assigned to the (110), (200), (210), (220), (240), (420), (520), and (001) facets, respectively (fig. S5, red curve and inset). We used density functional–based tight binding (DFTB) calculations to optimize the conformation of the 2D single layer and the configuration of different stacking models (17, 18). The energetically most favorable AA-stacking model yielded a PXRD pattern (fig. S5, pink curve) in good agreement with the experimentally observed profile. The Pawley-refined PXRD pattern (fig. S5, black curve) with the C2/m space group with unit-cell parameters of a = 34.4632 Å, b = 35.4951 Å, c = 3.7199 Å, α = γ = 90°, and β = 104.0277° reproduced the experimentally observed curve with negligible differences (fig. S5, green curve). Tables S1 and S2 summarize the atomistic coordinates generated by DFTB calculation and Pawley refinements, respectively. Thus, the reconstruction of sp²c-COF structure shows an extended 2D tetragon lattice with sp² carbon backbones along the x and y directions (Fig. 2A). The presence of the (001) facet at 24.7° suggests the structural ordering with 3.58-Å separation in the z direction perpendicular to the 2D sheets (Fig. 2B).

The sp²c-COF exhibited reversible nitrogen sorption isotherm curves with a Brunauer-Emmett-Teller surface area of 692 m² g⁻¹ (fig. S6A). The pore-size distribution profile revealed that sp²c-COF is microporous with a pore size of 1.88 nm (fig. S6B). This result is consistent with the lattice as revealed by the structural analysis.

Solid-state electronic absorption spectroscopy of sp²c-COF (fig. S7A, red curve) showed an absorption band at 498 nm, whose red shift of 53 nm from that of the model compound (fig. S7A, black curve, and scheme S1A) is indicative of extended π conjugation. In contrast, the imine-linked 2D COF (fig. S7A, blue curve; figs. S8 and S9; and scheme S1B), an analog to sp²c-COF, exhibited an absorption band blue-shifted 21 nm relative to sp²c-COF, indicating that the C=C linkage is more effective in transmission of π conjugation over the 2D lattice than that of the C=N bond. Moreover, the contrast in the optical colors (fig. S7B) between sp²c-COF (red), imine-linked 2D COF (yellow), and model compound (yellow-orange) also reflects the extended π conjugation in sp²c-COF. Cyclic voltammetry (CV) of sp²c-COF (fig. S10) revealed an oxidation potential at 0.94 V and a reduction potential at –0.96 V, indicating a narrow band gap of 1.90 eV. The highest occupied molecular orbital (HOMO) level was evaluated (19) as –5.74 eV, and the lowest unoccupied molecular orbital (LUMO) level was –3.84 eV, constituting a semiconductor band structure.

[1]Field of Energy and Environment, School of Materials Science, Japan Advanced Institute of Science and Technology, 1-1 Asahidai, Nomi 923-1292, Japan. [2]Department of Materials Molecular Science, Institute for Molecular Science, 38 Nishigo-naka, Myodaiji, Okazaki 444-8585, Japan. [3]School of Science and Technology, Nottingham Trent University, Clifton Lane, Nottingham NG11 8NS, UK. [4]Molecular Foundry and Advanced Light Source, Lawrence Berkeley National Laboratory, 1 Cyclotron Road, Mailstop 15R0317, Berkeley, CA 94720, USA. [5]Wilhelm-Ostwald-Institute for Physical and Theoretical Chemistry, Leipzig University, Linnéstrasse 2, 04103 Leipzig, Germany.
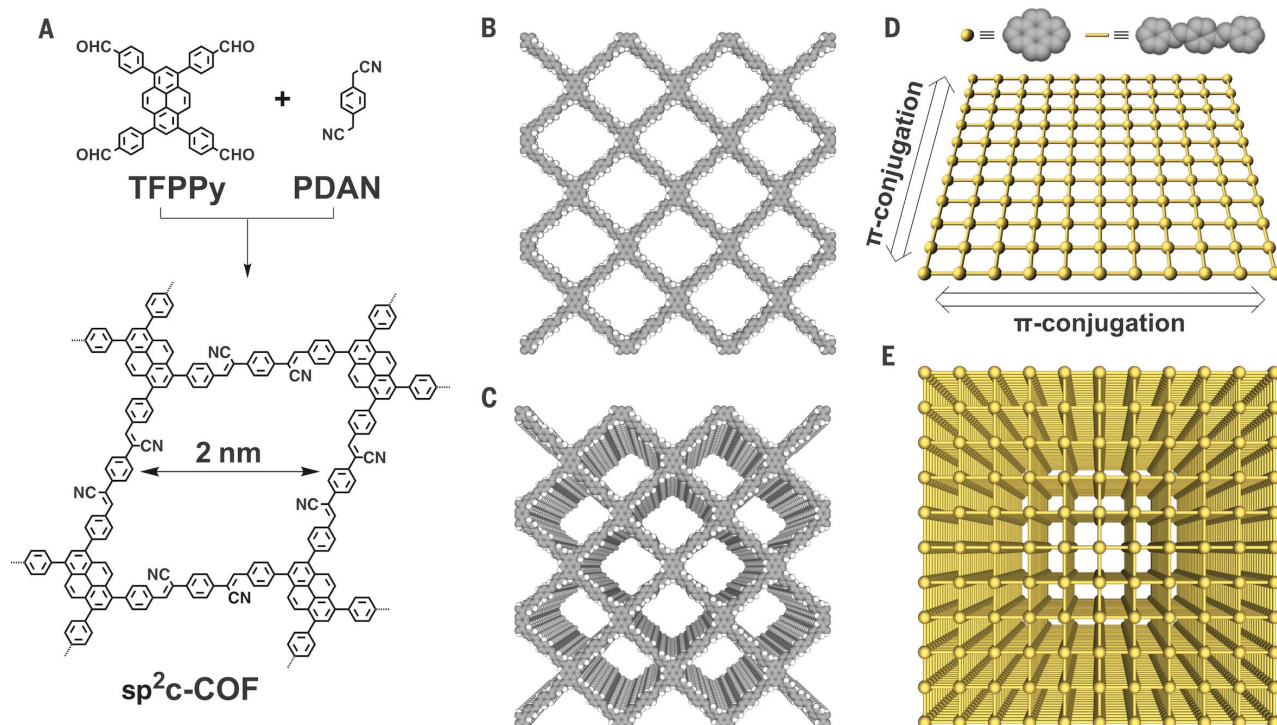*Corresponding author. Email: djiang@jaist.ac.jp

Fig. 1. Chemical and lattice structures of a crystalline porous sp² carbon framework. (**A**) Schematic representation of the synthesis of the crystalline porous sp²-hybridized carbon covalent organic framework (sp²c-COF) with pyrene knots and phenylenevinylene linkers connected by C=C bonds (one pore is shown). TFPPy, tetrakis(4-formylphenyl)pyrene; PDAN, 1,4-phenylenediacetonitrile. (**B** and **C**) Reconstructed crystal structures of (B) one layer and (C) many layers of the 2D sp²c-COF (three-by-three unit cell). The pyrene knots are regularly interweaved in a 2-nm pitch along the x and y directions and are stacked at an interval of 3.58 Å along the z direction via π-π interactions to form ordered pyrene knot π arrays and 1D channels. (**D** and **E**) Ball (pyrene knot) and stick (phenylenevinylene chain) representations of (D) a 2D sheet with extended π conjugations along the x and y directions and (E) the stacked sp²c-COF.
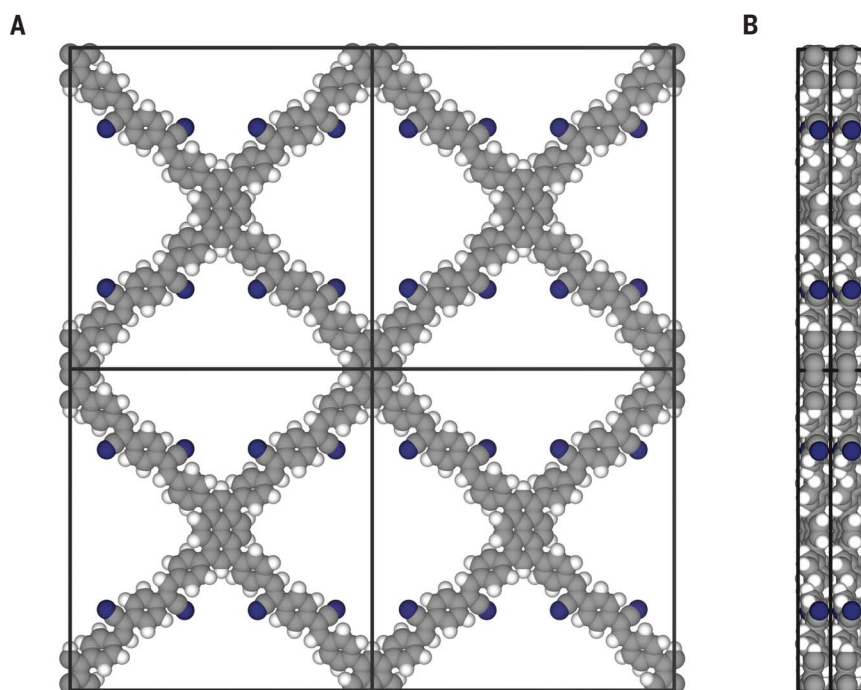

Fig. 2. Crystal structure. (**A** and **B**) Reconstructed crystal structure at top (A) and side (B) views. The 2D layers are stacked at a 3.58-Å interval along the z direction.

The sp²c-COF solid samples were chemically oxidized by iodine and pressed to make thin discs with a thickness of 0.08 cm. The electrical conductivity was measured across a 0.2-cm-width Pt gap electrode under air at 25°C. The iodine-doped sp²c-COF exhibited a linear current-voltage (*I-V*) profile indicative of ohmic conduction (fig. S11, red curve). The slope yielded a conductivity of 7.1 × 10^{-2} S m^{-1}. The pristine COF sample was an insulator with a conductivity of only 6.1 × 10^{-14} S m^{-1} (fig. S11, black curve).

To investigate the feature of radical species in the 2D sp² carbon framework, we monitored the doping process of the COF samples in the presence of iodine vapor under iodine-saturated pressure in a sealed quartz tube with electron spin resonance (ESR) spectroscopy (Fig. 3). An ESR signal appeared at *g*-factor = 2.003, just after 3 min of iodine doping (Fig. 3A). The peak-to-peak height increased and leveled off after 1 day of doping (Fig. 3B). The increase in ESR intensity with iodine doping indicates that the charge carriers generated also possess a spin degree of freedom. The ESR linewidth and resonance field (*g*-factor) were almost constant regardless of the doping level; the shift of the *g*-factor from that of the free electron (*g* = 2.0023) was very small. The ESR linewidth of 0.13 mT indicates that the sp² carbon lattice is free of anisotropic *g*-tensor and hyperfine interactions.
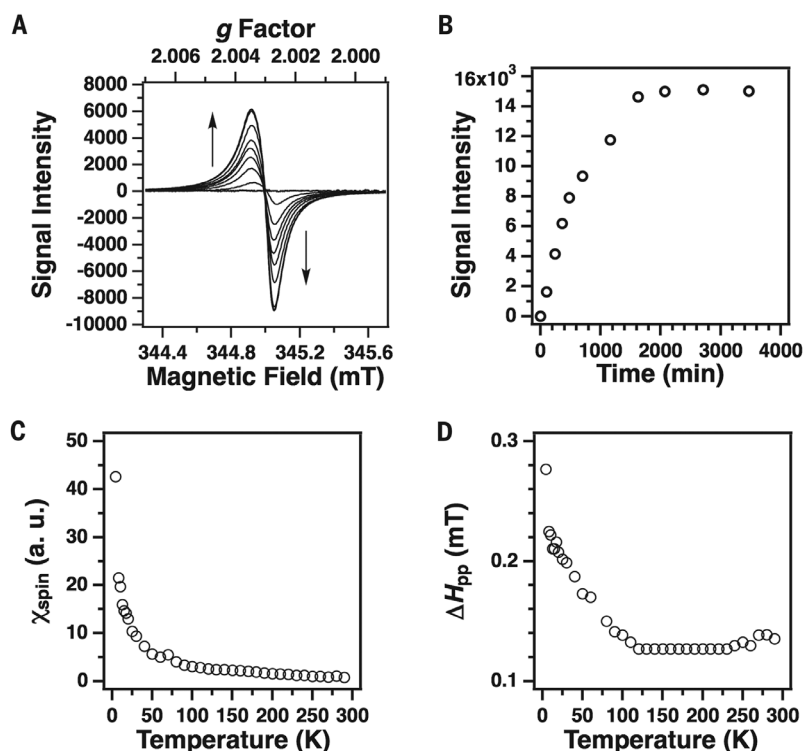
Fig. 3. ESR studies. (**A**) Time evolution of the electron spin resonance (ESR) spectra upon iodine doping. (**B**) Plot of the peak-to-peak height of the ESR signals versus doping time. The peak intensity was saturated after 26 hours and did not decrease after doping. (**C**) Temperature dependency of the spin susceptibility (χ_{spin}) for the iodine-doped sp²c-COF. a. u., arbitrary units. (**D**) Temperature dependency of the ESR linewidth (ΔH_{pp}).

These results suggest that the frontier electrons maintain to locate at the pyrene knots and do not form nonradical bipolarons.

The temperature dependence of the spin susceptibility χ_{spin} determined by integrating the ESR signal intensity (Fig. 3C) shows that the *g*-factor was temperature independent. The Curie-like enhancement of the χ_{spin} value indicates that the existing spin freedom persists to the low temperature (Fig. 3C). Figure 3D shows the temperature dependency of the ESR linewidth, ΔH_{pp}. The ESR linewidth is almost constant above 100 K. The temperature-independent ESR linewidth is dominated by the spin-spin exchange interaction through space between spins in neighboring layers and indicates the localized nature of the spins at the pyrene knots. Considerable exchange interaction between spins is an evidence for the high density of spins generated in the iodine-doped sp²c-COF. The ESR linewidth gradually increased below 100 K, suggesting that long-range magnetic order developed in the framework. Such a 2D spin structure is inaccessible by either 1D conjugated polymers (*20*, *21*) or conventional 2D COFs (*1*).

The absence of bipolarons observed for sp²c-COF is totally different from 1D conjugated polymers, which eventually form bipolarons without spins and greatly diminish the spins in the doped materials (*22–25*). We compared the ESR spectra with those of 1D sp²-polymer (scheme S2) and C=N-linked 2D COFs upon iodine doping, which gave rise to only very weak ESR signals (fig. S12). The ESR intensities of sp²c-COF were 120 and 25 times higher than those of 1D sp²c-polymer and C=N-linked 2D COFs at room temperature, respectively. The fully π-conjugated sp² carbon 2D lattice is essential for generating high-density radicals in the materials. Moreover, we used wide-angle x-ray scattering (WAXS) to investigate the structure of crystalline sp²c-COF upon iodine doping (*26*, *27*). The WAXS peaks were unchanged before and after prolonged iodine doping with respect to the (110), (200), (210), (220), (240), (420), and (001) facets (fig. S13), indicating that the pyrene arrays are retained upon chemical oxidation.

To verify that the observed long-range order was intrinsic, we used superconducting quantum interference device (SQUID) magnetometry to perform magnetic susceptibility measurements. Figure 4A shows the temperature dependence of the magnetic susceptibility (χ). The spin susceptibilities determined by both ESR and SQUID measurements were in agreement in the entire temperature range. Above 100 K, the spins were paramagnetic and randomly oriented in the material. The magnetic susceptibility was greatly enhanced below 100 K. By using the magnetic susceptibility below 30 K and assuming $S = 1/2$ spin, the spin concentration and the Weiss temperature (Θ) were estimated to be 0.7 per pyrene

unit and 8.1 K, respectively. Therefore, iodine-doped sp²c-COF with exceptionally dense spins is a bulk magnet.

Magnetization (*M*)–applied field (*H*) relations revealed that sp²c-COF yielded linear curves at the temperatures above 20 K; below 10 K, the *M-H* plots became nonlinear (Fig. 4B, blue and red curves). The nonlinearity denotes a ferromagnetic phase transition, whereas the spin-spin coherence is developed with unidirectionally aligned spins across the material (Fig. 4C).

As controls, we investigated the electronic and magnetic behaviors of the model compound, a 1,6-linear polymer (scheme S3), and an amorphous version of sp²c-COF referred to as sp²c-CMP (CMP, conjugated microporous polymer) (scheme S4). sp²c-CMP has the same components as sp²c-COF but does not possess ordered layer structure (fig. S14, A to C). The 1,6-linear polymer exhibited an absorption band at 446 nm (fig. S15) and an electronic bandgap of 2.34 eV (fig. S16B and table S3). The sp²c-CMP sample exhibited an adsorption band at 436 nm (fig. S15), which is blue-shifted by 62 nm from that of sp²c-COF (498 nm). From the adsorption spectrum, the optical band gap of sp²c-CMP was evaluated to be 2.01 eV, whereas its electronic band gap was 1.96 eV (fig. S16C and table S3), according to the CV measurements. Upon doping with iodine, the model compound exhibited a conductivity of only 4.1×10^{-8} S m^{-1} (fig. S17A) and an ESR intensity equal to 1/100 that of sp²c-COF (fig. S18, A and B). The spin density is negligible (fig. S19, A and B). Upon doping, the model compound did not exhibit magnetic state transition and magnetic field response from the *M-H* curve (fig. S20A). The 1,6-linear polymer, upon doping with iodine, exhibited a conductivity of 2.9×10^{-7} S m^{-1} (fig. S17B). From the time-dependent ESR measurements (fig. S18C), the saturated ESR intensity is 1/406 that of sp²c-COF (fig. S18A). The 1,6-linear polymer had a spin density of only 0.004 per pyrene unit (fig. S19, A and C) and did not exhibit magnetic state transition and magnetic field response (fig. S20B). The sp²c-CMP samples, upon doping with iodine, exhibited a conductivity of 8.1×10^{-3} S m^{-1} (fig. S17C), which is one order of magnitude lower than that of sp²c-COF. The time-dependent ESR measurements revealed signals at $g = 2.003$ (fig. S18D). However, the saturated ESR intensity is only 1/5 that of sp²c-COF (fig. S18A). The spin density is 0.057 per pyrene unit (fig. S19, A and D). These results indicate that the amorphous sp²c-CMP cannot form a dense spin system. The SQUID measurements revealed that a small amount of part of sp²c-CMP is paramagnetic at room temperature and shows a trace of superparamagnetism at low temperature (fig. S20C, $\Theta = 1.5$ K), as indicated by the decreased magnetism after the field of 40,000 Oe (red curve). In contrast, the ferromagnetism with increasing magnetism is an overwhelming majority in sp²c-COF with saturated magnetism after the field of 40,000 Oe (Fig. 4B, red curve). These results confirmed that the observed electronic and spin functions are inherent to sp²c-COF and originate from its extended crystalline structure.
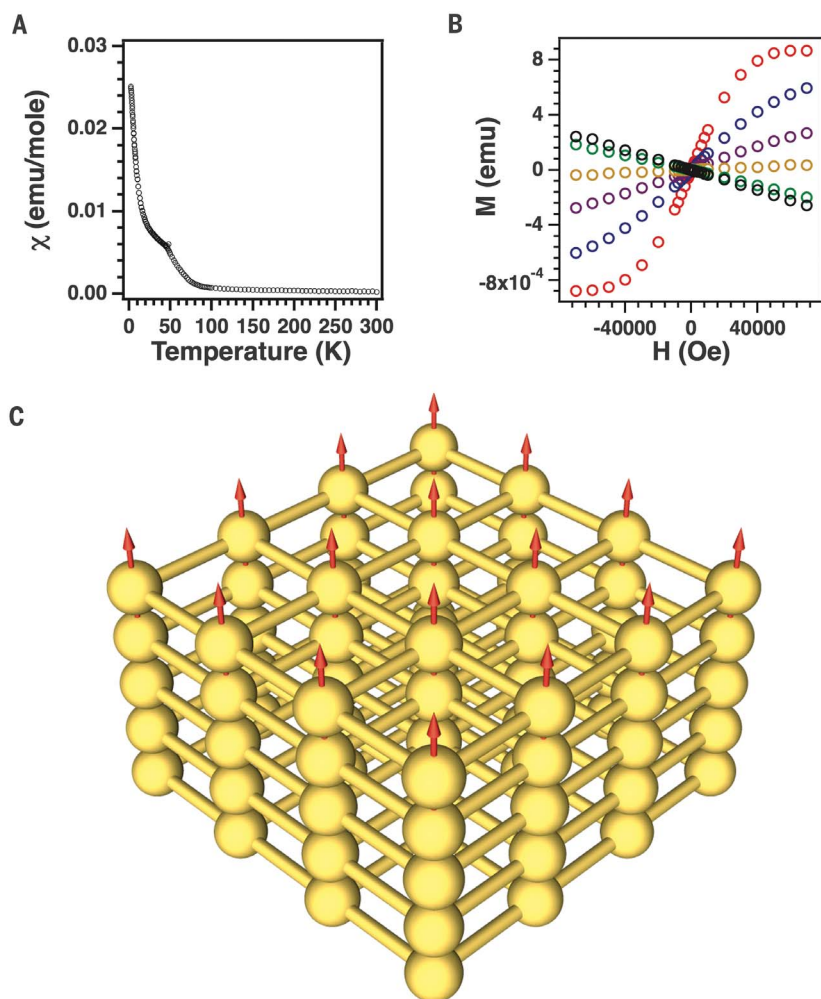
Fig. 4. Magnetization and spin alignment. (**A**) Temperature dependence of the spin susceptibility, χ, determined by the superconducting quantum interference device (SQUID) magnetometer for the iodine-doped sp^2c-COF. emu, electromagnetic units. (**B**) Magnetic (M)-applied field (H) profiles at different temperatures (red, 2 K; blue, 5 K; purple, 10 K; brown, 20 K; green, 100 K; black, 300 K). The nonlinearity of the curves denotes the ferromagnetic phase transition. (**C**) Schematic of spin alignment in sp^2c-COF (three-by-three lattice). Red arrows represent spins. The spins are isolated at the knots and are unidirectionally aligned across the framework via ferromagnetic phase transition to develop spin-spin coherence.

REFERENCES AND NOTES

1. N. Huang, P. Wang, D. Jiang, *Nat. Rev. Mater* **1**, 16068 (2016).
2. Y. Xu, S. Jin, H. Xu, A. Nagai, D. Jiang, *Chem. Soc. Rev.* **42**, 8012–8031 (2013).
3. J.-X. Jiang et al., *Angew. Chem. Int. Ed.* **46**, 8574–8578 (2007).
4. D. T. Mowry, *J. Am. Chem. Soc.* **67**, 1050–1051 (1945).
5. H. E. Zimmerman, L. Ahramjian, *J. Am. Chem. Soc.* **81**, 2086–2091 (1959).
6. S. Patai, Y. Israeli, *J. Chem. Soc.* **0**, 2025–2030 (1960).
7. D. A. M. Egbe et al., *Macromolecules* **37**, 8863–8873 (2004).
8. P. J. Waller, F. Gándara, O. M. Yaghi, *Acc. Chem. Res.* **48**, 3053–3063 (2015).
9. J. W. Colson et al., *Science* **332**, 228–231 (2011).
10. L. Ascherl et al., *Nat. Chem.* **8**, 310–316 (2016).
11. S. Kandambeth et al., *J. Am. Chem. Soc.* **134**, 19524–19527 (2012).
12. M. R. Rao, Y. Fang, S. De Feyter, D. F. Perepichka, *J. Am. Chem. Soc.* **139**, 2421–2427 (2017).
13. X.-H. Liu et al., *J. Am. Chem. Soc.* **135**, 10470–10474 (2013).
14. X. Zhuang et al., *Polym. Chem.* **7**, 4176–4181 (2016).
15. Materials and methods, figs. S1 to S7, and tables S1 and S2 are available as supplementary materials.
16. B. C. Thompson, Y.-G. Kim, T. D. McCarley, J. R. Reynolds, *J. Am. Chem. Soc.* **128**, 12714–12725 (2006).
17. B. Aradi, B. Hourahine, T. Frauenheim, *J. Phys. Chem. A* **111**, 5678–5684 (2007).
18. www.dftb.org
19. $E_{HOMO} = -e(E_{oxidation, onset} + 4.8 - E_{Fc/Fc+})$; $E_{LUMO} = -e(E_{reduction, onset} + 4.8 - E_{Fc/Fc+})$, where E_{HOMO} is the HOMO energy level, E_{LUMO} is the LUMO energy level, e is an electron particle, $E_{oxidation, onset}$ and $E_{reduction, onset}$ are the onset oxidation and reduction potentials, respectively, and $E_{Fc/Fc+}$ is the potential of a ferrocene/ferricenium ion couple as external standard, measured under the same conditions.
20. J. L. Bredas, G. B. Street, *Acc. Chem. Res.* **18**, 309–315 (1985).
21. S. Kuroda, K. Marumoto, Y. Shimoi, S. Abe, *Thin Solid Films* **393**, 304–309 (2001).
22. A. Sakamoto, Y. Furukawa, M. Tasumi, *J. Phys. Chem.* **98**, 4635–4640 (1994).
23. I. Orion, J. P. Buisson, S. Lefrant, *Phys. Rev. B* **57**, 7050–7065 (1998).
24. W. R. Salaneck, R. H. Friend, J. L. Brédas, *Phys. Rep.* **319**, 231–251 (1999).
25. R. R. Chance, J. Bredas, R. Silbey, *Phys. Rev. B* **29**, 4491–4495 (1984).
26. A. Hexemer et al., *J. Phys. Conf. Ser.* **247**, 012007 (2010).
27. J. Ilavsky, *J. Appl. Cryst.* **45**, 324–328 (2012).

Science

Two-dimensional sp^2 carbon–conjugated covalent organic frameworks

Enquan Jin, Mizue Asada, Qing Xu, Sasanka Dalapati, Matthew A. Addicoat, Michael A. Brady, Hong Xu, Toshikazu Nakamura, Thomas Heine, Qiuhong Chen and Donglin Jiang

Conjugated covalent networks

Although graphene and related materials are two-dimensional (2D) fully conjugated networks, similar covalent organic frameworks (COFs) could offer tailored electronic and magnetic properties. Jin *et al.* synthesized a fully π-conjugated COF through condensation reactions of tetrakis(4-formylphenyl)pyrene and 1,4-phenylenediacetonitrile. The reactions were reversible, which provides the self-healing needed to form a crystalline material of stacked, π-bonded 2D sheets. Chemical oxidation of this semiconductor with iodine greatly enhanced its conductivity, and the radicals formed on the pyrene centers imparted a high spin density and paramagnetism.
Science, this issue p. 673

ARTICLE TOOLS	http://science.sciencemag.org/content/357/6352/673
SUPPLEMENTARY MATERIALS	http://science.sciencemag.org/content/suppl/2017/08/16/357.6352.673.DC1
REFERENCES	This article cites 28 articles, 1 of which you can access for free http://science.sciencemag.org/content/357/6352/673#BIBL
PERMISSIONS	http://www.sciencemag.org/help/reprints-and-permissions

Use of this article is subject to the Terms of Service